Supporting Information for

Upconversion-Chameleon-Driven DNA Computing: DNA-Unlocked Inner-Filter-Effect (DU-IFE) for Operating Multicolor Upconversion Luminescent DNA Logic Library and Its Biosensing Application

Daoqing Fan,[ab] Erkang Wang [ab] and Shaojun Dong [ab]**

[a] State Key Laboratory of Electroanalytical Chemistry, Changchun Institute of Applied Chemistry, Chinese Academy of Sciences, Changchun, Jilin, 130022 (China)

[b] University of Chinese Academy of Sciences, Beijing, 100039 (China).

E-mail: dongsj@ciac.ac.cn; ekwang@ciac.ac.cn.

This ***Supporting Information*** includes:

Table S1.

Figure S1-S16.

Table and Figures.

Table S1. Sequences of DNAs used in this work. The split-G4 parts were colored in red.

Devices	Names	Sequences (5' to 3')
YES	T30695 (TG4)	GGGTGGGTGGGTGGGT
AND	G3	ACTAGAATCTGTCA GGGTAGGGCGGG
	G1	TGGGT TGACAGATTCTAGT
OR	TG4	*See the first line*
	PW_{17}	GGGTAGGGCGGGTTGGG
INH	TG4	*See the first line*
	C4	ACCCACCCACCCACCC
XOR	RP	ATACAGTAATAG GGGTGGG ATAAGAAAGTACAA
	RA	TGGGTGGG CTATTACTGTAT
	CA	ATACAGTAATAG CCCA
	RB	TTGTACTTTCTTAT GGGTGGGT
	CB	ACCC ATAAGAAAGTACAA
MAJ	JA	GGG CGATGTTCGT ACATTCAGTA GGG
	JB	GGG GACTATCGTT GTCGTTGTAG GGG
	JC	GGG TTCGCGGATT GTGCGTCACT GGG
	P1	ACGAACATCG GGGTGGG CTACAACGAC
	P2	AACGATAGTC GGGTGGG AGTGACGCAC
	P3	AATCCGCGAA GGGTGGG TACTGAATGT
Encoder	TG4	*See the first line*
	T30	$(TTTTT)_6$
Parity checker	TG4	*See the first line*
	T20	$(TTTTT)_4$
	T30	$(TTTTT)_6$
	T40	$(TTTTT)_8$
DNA caliper	Da	GACGTAATAGT GGGTAGGGCGGG
	Db	TGGGT GAGATGTATG
	D0	CATACATCTC CTATTACGTC
	D3	CATACATCTC TTT CTATTACGTC
	D5	CATACATCTC TTGTT CTATTACGTC
	D7	CATACATCTC TTGACTT CTATTACGTC
	D13	CATACATCTC TTTTTGACTTTTT CTATTACGTC

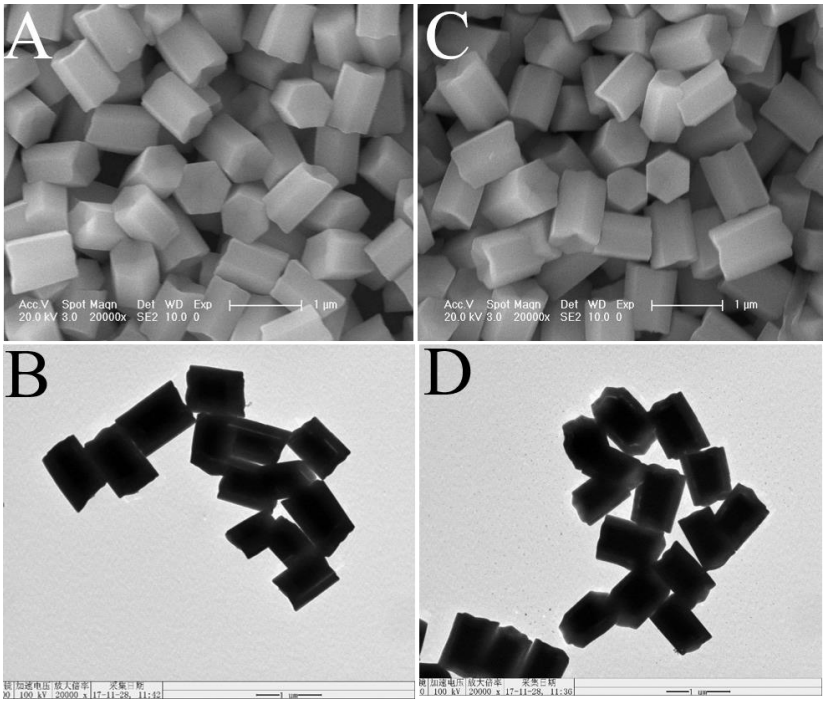

Figure S1. (A) SEM and **(B)** TEM images of UCNPs ($NaYF_4$: 18%Yb/2%Er); **(C)** SEM and **(D)** TEM images of UCNPs ($NaYF_4$:18%Yb/2%Er/5%Tm). The scale bars were all 1 μm.

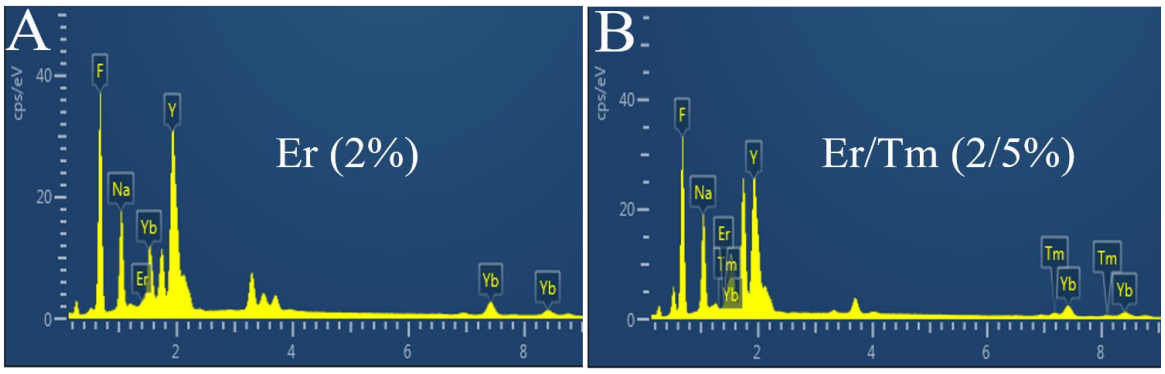

Figure S2. Element distribution spectra (EDS) of **(A)** Er-doped and **(B)** Er/Tm-codoped UCNPs.[S1]

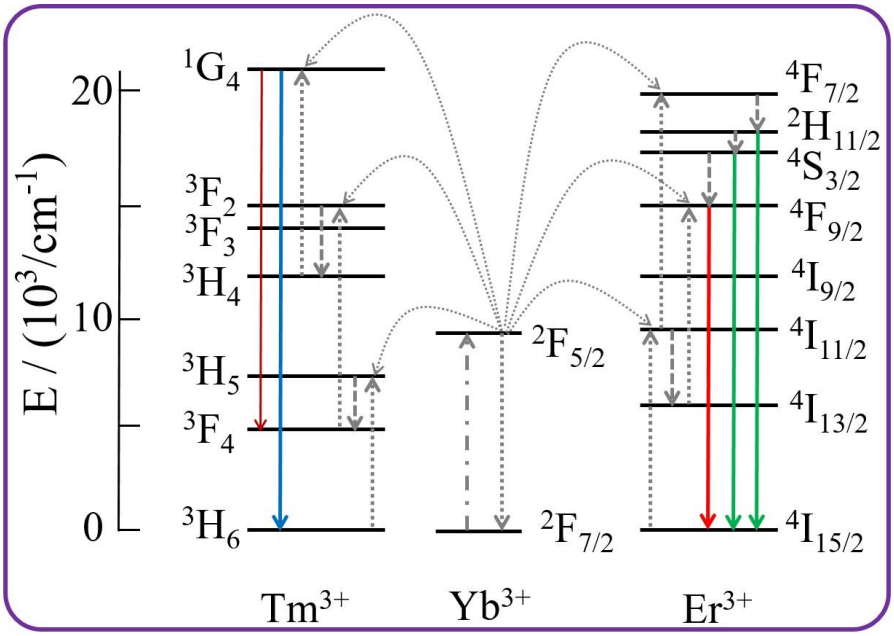

Figure S3. Detailed UCL mechanism between Tm^{3+}, Yb^{3+} and Er^{3+} under 980 NIR-laser. [S6] The *dashed-dotted, dashed, dotted and full arrows* represent the photon excitation, multi-photon relaxation, energy-transfer and emission procedures, respectively.

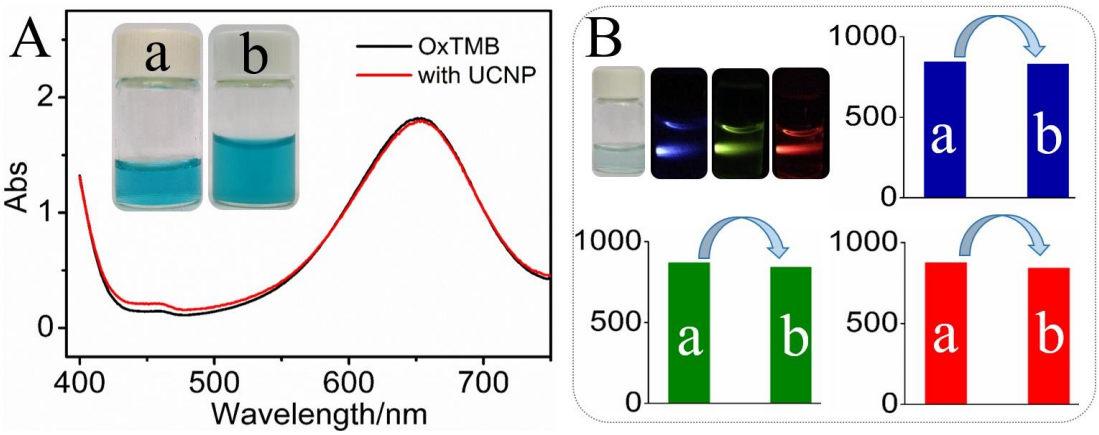

Figure S4. (A) Absorbance spectra of OxTMB and the mixture of OxTMB/UCNPs (red line was multiplied by two times as for the doubled-volumes of OxTMB/UCNPs than OxTMB) and visual photos (inset, (a) OxTMB, (b) OxTMB/UCNPs), OxTMB's concentration was calculated as 46.15 μM via A=εbc, ε_{OxTMB}=39000 $M^{-1}cm^{-1}$, b=1 cm; **(B)** Visual photos of oxidation product of TMB that catalyzed by non-G4 strands/hemin and UCL photos after mixing above product with tricolor UCNPs and corresponding UCL peak intensity changes: **(a)** original intensities and **(b)** that after adding above product, blue (480 nm), green (550 nm) and red (665nm) colors represent different UC emissions.

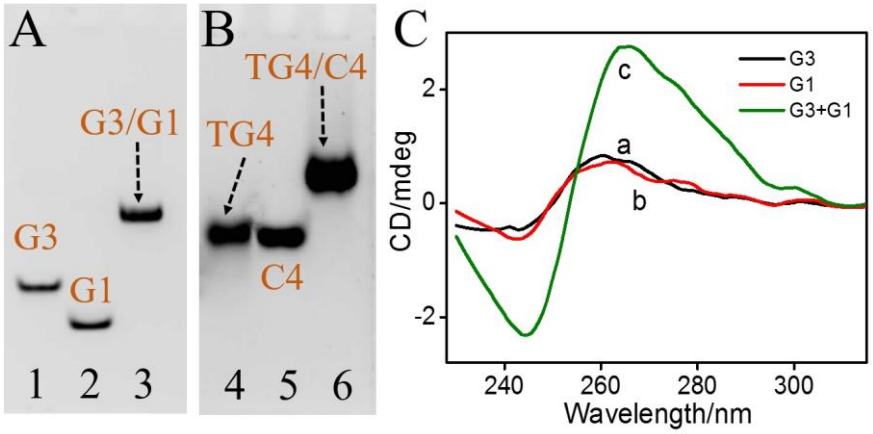

Figure S5. (A) The PAGE results of strands G3, G1 and **(B)** that of TG4, C4; **(C)** CD spectra of strands G3 and G1.

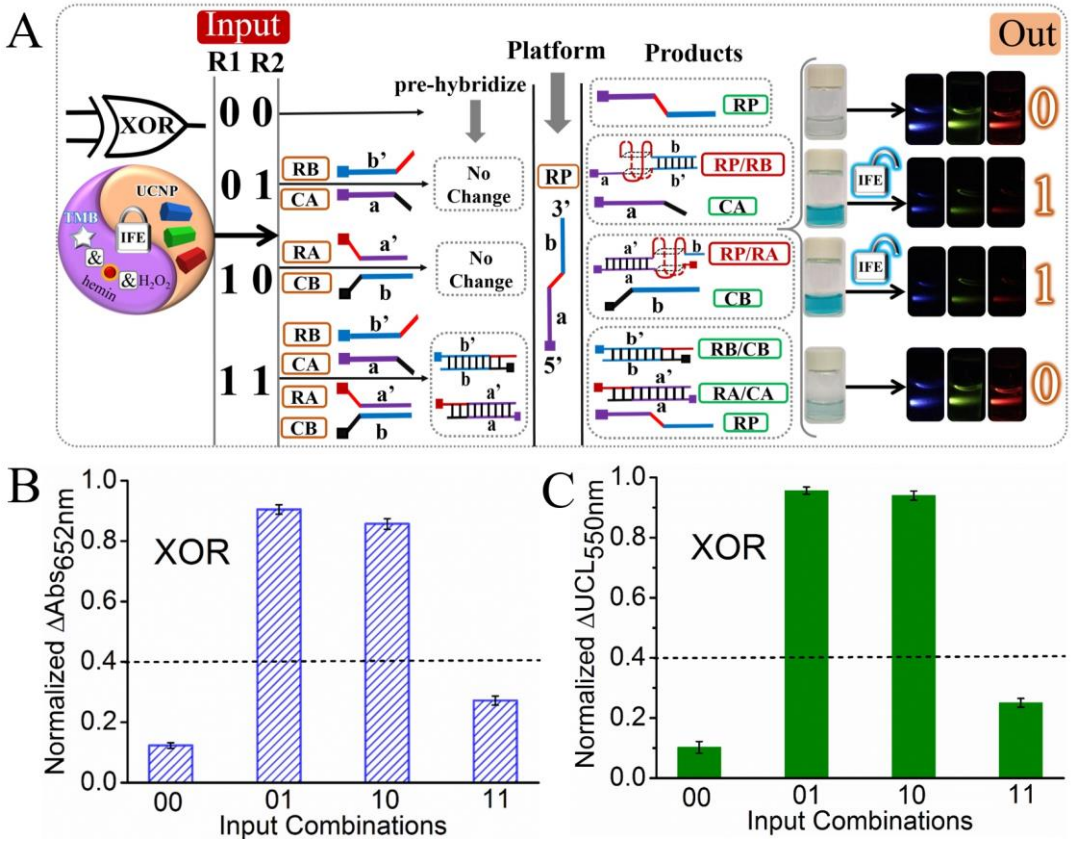

Figure S6. (A) Operation of the XOR gate based on DU-IFE, R1 (mixture of strands RA, CB), R2 (mixture of strands RB, CA) were inputs and RP was platform. (5' ends of DNAs were squared, poly-G regions were colored in red, and G4 was illustrated with red-basket structure); **(B)** Normalized ΔAbs column bars of XOR gate under different input combinations; **(C)** Normalized ΔUCL column bars of XOR gate ($UCL_{550\ nm}$) under different input combinations. "01" represents the absence of R1 and presence of R2, others ditto.

RP (integrated with GGGTGGG (red region) in the middle) was the platform of XOR gate. The mixture of strand RA+CB and that of RB+CA was input R1 and R2, respectively. As shown in **Figure S6A**, the purple part (a') of RA (with $(TGGG)_2$ at 5' end, red region) could hybridize with the purple part of XP (a) to form complete G4 (RP/RA). N-methyl mesoporphyrin IX (NMM) was applied to testify G4's formation. The unique circular dichorism (CD) peaks **(Figure S7A)** and obviously enhanced fluorescence intensity at 610 nm of NMM in the presence of RP and RA (**Figure S7B**) indicated the formation of parallel-G4. [S2-S5] Analogously, strand RB can also hybridize with blue part (b) of RP to form complete G4 (RP/RB), **Figure S8A**. By contrast, the purple part (a) of CA (with CCCA at 3' end, green region) could hybridize with RA to produce more stable [S2-S5] RA/CA, indicating that the pre-hybridization between RA and CA will inhibit the formation of G4 (RP/RA), inset of **Figure S7B**. Similarly, the pre-hybridization between RB and CB will also inhibit the formation of G4 (RP/RB). While, the mix of CB and RA (or the mix of CA and RB) will influence neither the reaction between RP and RA (or RB) nor the formation of G4, **Figure S8B**. Corresponding PAGE verification can be found in our previous work. [S3]

On the basis of above DNA hybridizations, the G4zyme was alternately formed after reacted with hemin under different inputs combinations. The incomplete G4zyme can't initiate the DU-IFE and produce output "0". By contrast, complete G4zyme will initiate the DU-IFE and produce output "1", **Figure S6B, C.**

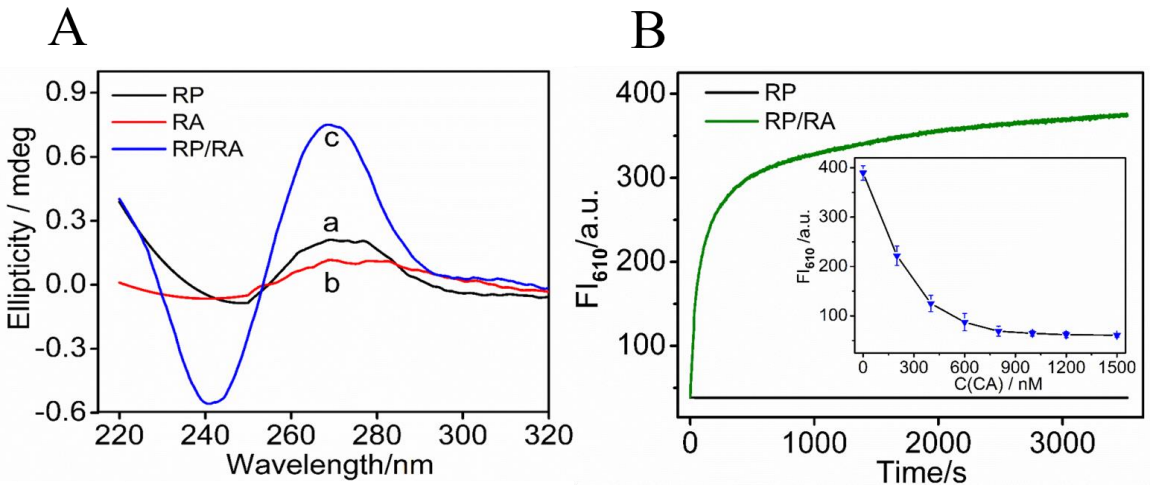

Figure S7. (A) CD spectra of strands RP, RA; **(B)** Fluorescent kinetics of NMM at 610nm, inset was the optimization of CA's concentration.

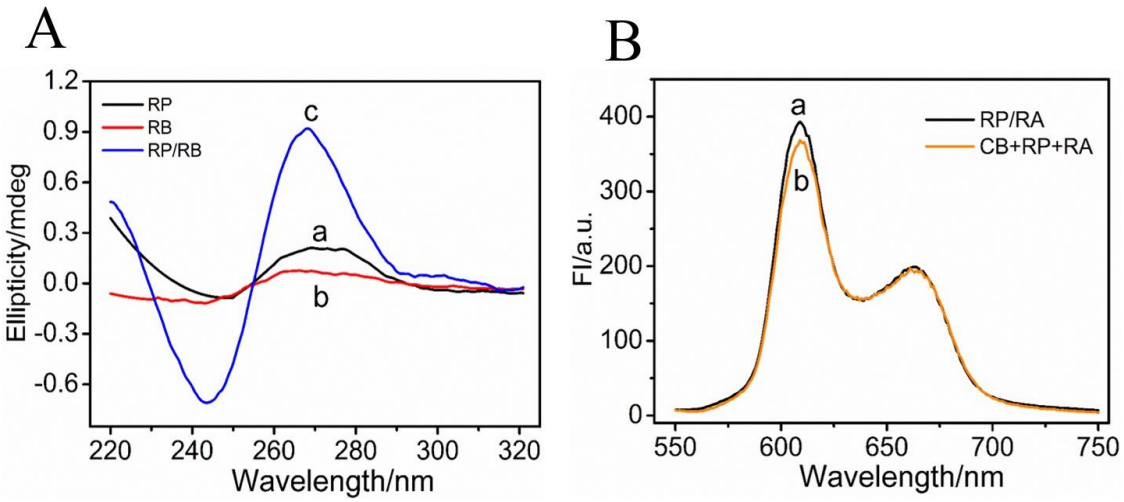

Figure S8. **(A)** CD spectra of strands RP, RB; **(B)** Fluorescence spectra of NMM in the presence of different strands.

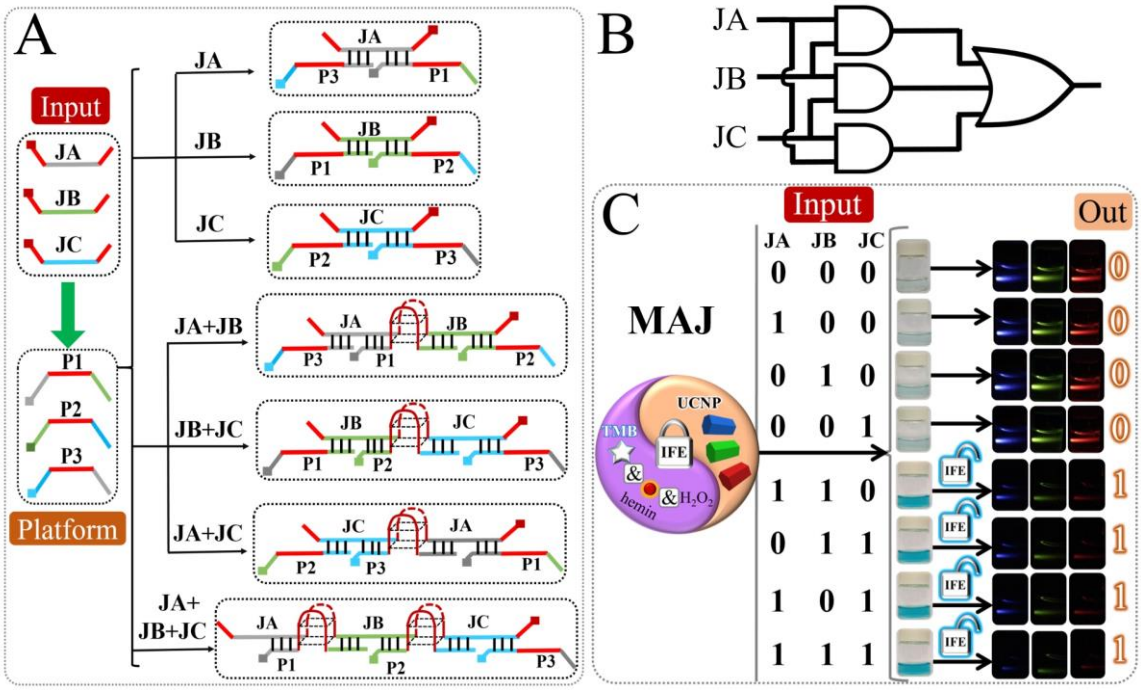

Figure S9. (A) Detailed hybridizations between different strands used in the MAJ gate, strands JA, JB and JC were inputs and the mixture of P1, P2 and P3 was platform. (5' ends of all the DNAs were squared, poly-G regions were colored in red and G4 was illustrated with red-basket structure); **(B)** Equivalent logic symbols of MAJ gate; **(C)** Operation of the MAJ gate based on DU-IFE under different input combinations.

The middle region of platform DNAs were integrated with GGGTGGG and the 3' and 5' ends of each input DNA were integrated with GGG, respectively. Through reasonable design, the right part of JC can hybridize with P3's left part (pale-blue region), and the left part of JC can complement with P2's right part (pale-blue region), while JC does not interact with P1. JA could bridge P1 and P3 together while not interact with P2, and JB could bridge P1 and P2 together while not hybridize with P3 **(Figure S9A)**. The DNA hybridizations were adequately verified by corresponding PAGE results **(Figure S10, B-D)**. Thus, the formation of G4 can be easily modulated via above DNA hybridizations. With the addition of one input, no G4 is produced. While, in the presence of any two inputs, the complete G4 will form **(Figure S10A)**. And more G4 can be acquired in the presence of all three inputs.

Based on above DNA hybridizations, the G4zyme can be alternately produced after mixed with hemin under various inputs variations. The incomplete G4zyme can't unlock DU-IFE and generate output "0". In comparison, complete G4zyme will unlock DU-IFE and generate output "1", **Figure S11**.

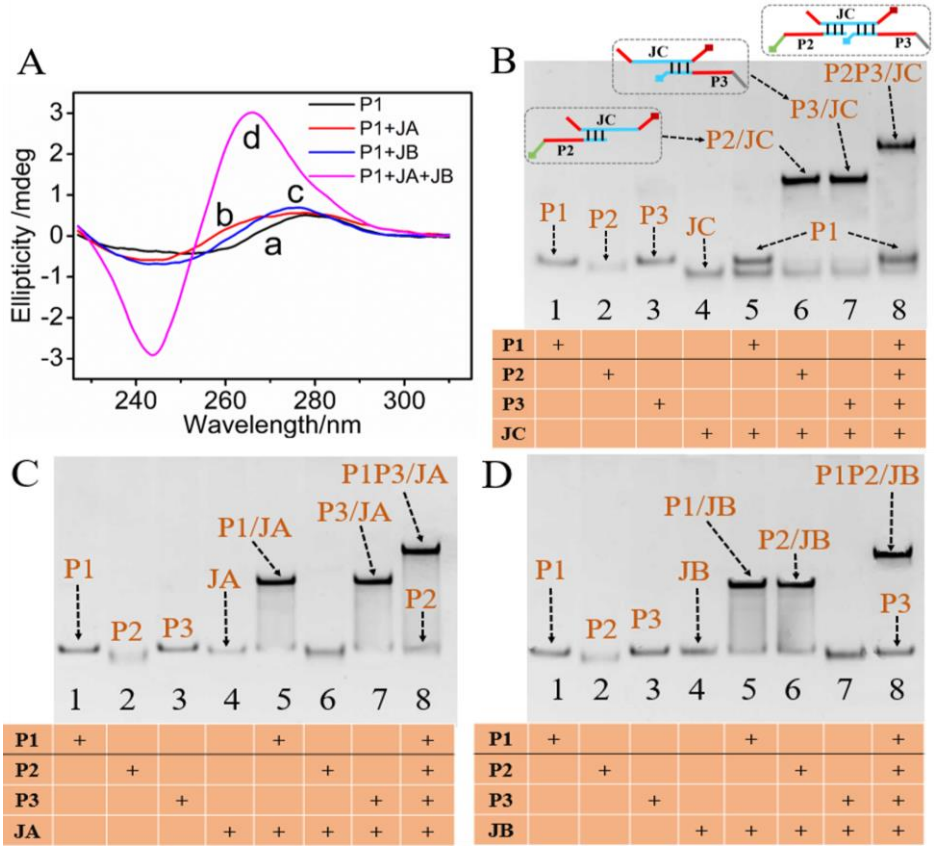

Figure S10. (A) CD spectra of P1, P1+JA. P1+JB and P1+JA+JB; **(B)** 15% PAGE analysis of the interactions between strands P1, P2, P3 and JC; **(C)** The interactions between strands P1, P2, P3 and JA; **(D)** The interactions between strands P1, P2, P3 and JB. The presence of strand was illustrated with "+", the duplexes were attached with corresponding graphics in **(B)**.

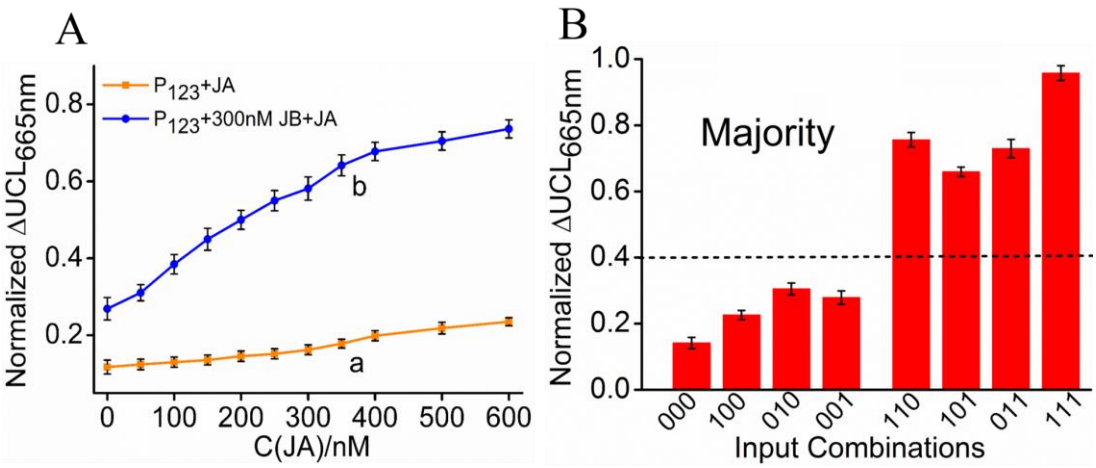

Figure S11. (A) Optimization of the concentrations of strand JA, 300 nM P1/P2/P3 and 300 nM JB were kept as constant; **(B)** Normalized ΔUCL column bars of MAJ gate (UCL_{665nm}) under different input combinations. "100" represented the presence of JA and absence of JB, JC, others ditto.

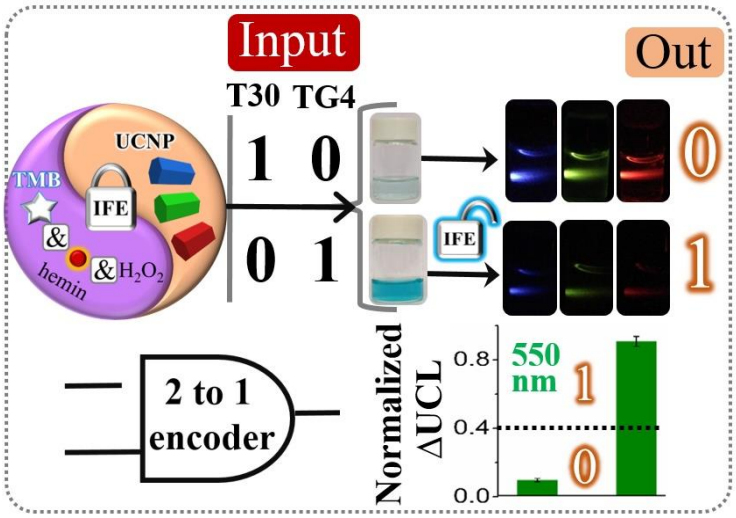

Figure S12. Operation of the 2 to 1 encoder based on DU-IFE, strands T30 and TG4 were two inputs.

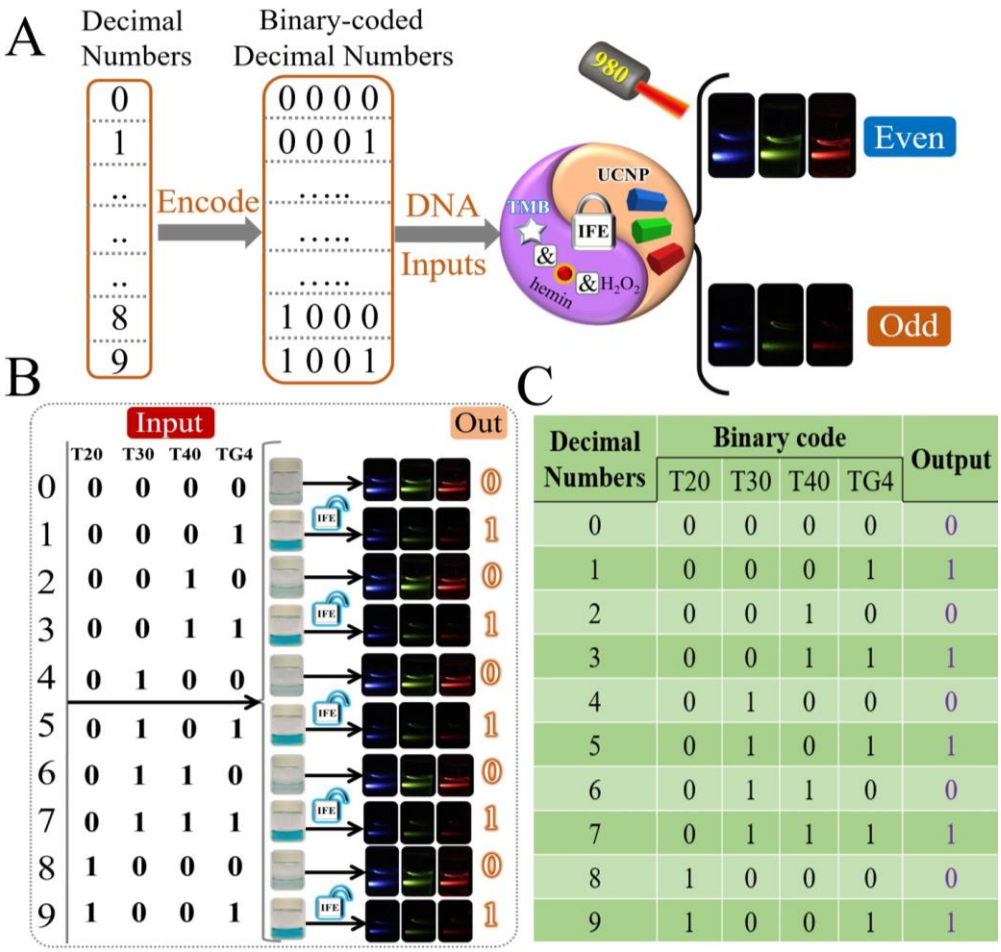

Decimal Numbers	Binary code				Output
	T20	T30	T40	TG4	
0	0	0	0	0	0
1	0	0	0	1	1
2	0	0	1	0	0
3	0	0	1	1	1
4	0	1	0	0	0
5	0	1	0	1	1
6	0	1	1	0	0
7	0	1	1	1	1
8	1	0	0	0	0
9	1	0	0	1	1

Figure S13. Operation of the parity-checker for discriminating natural numbers (from 0 to 9) based on DU-IFE, strands T20, T30, T40 and TG4 were inputs.

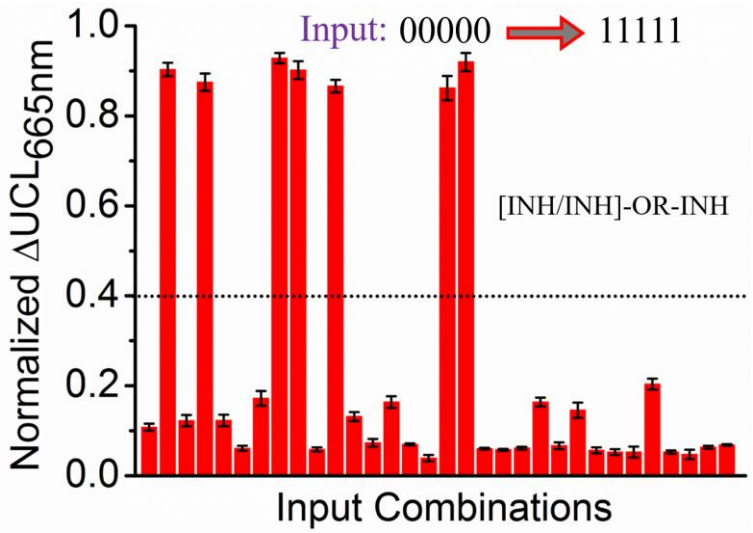

Figure S14. Normalized ΔUCL column bars of the 5-input concatenated circuit [INH/INH]-OR-INH under different input combinations. UCL_{665nm} was applied as example. The 5 inputs were RA, CA, RB, CB and GSH. "00001" represented the absence of RA, CA, RB, CB and presence of GSH, others ditto.

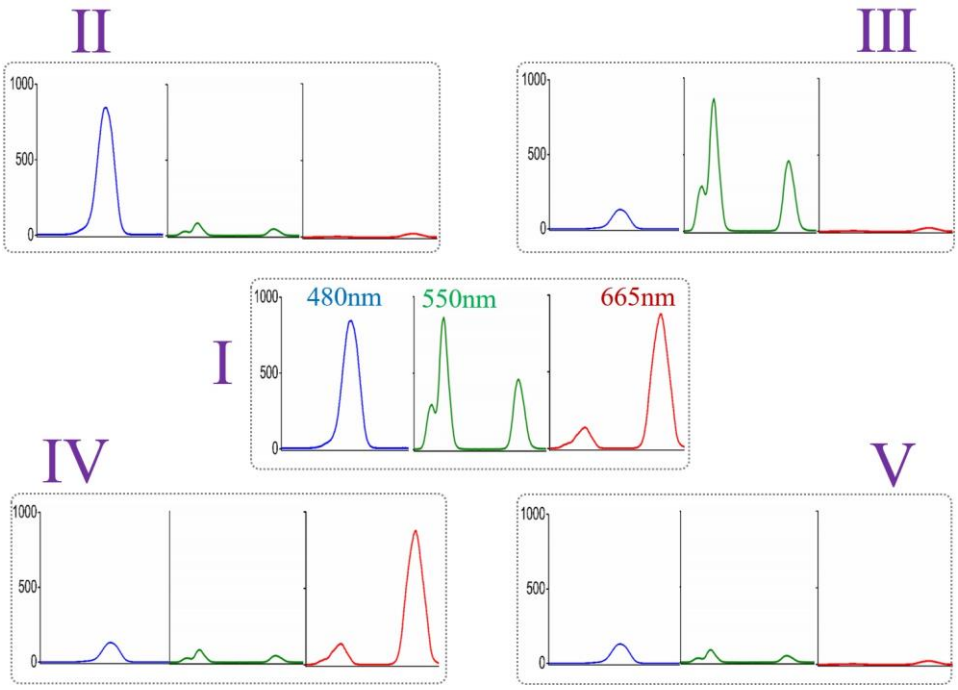

Figure S15. UCL spectra of the molecular tricolor-signal-light under different 5 color-states.

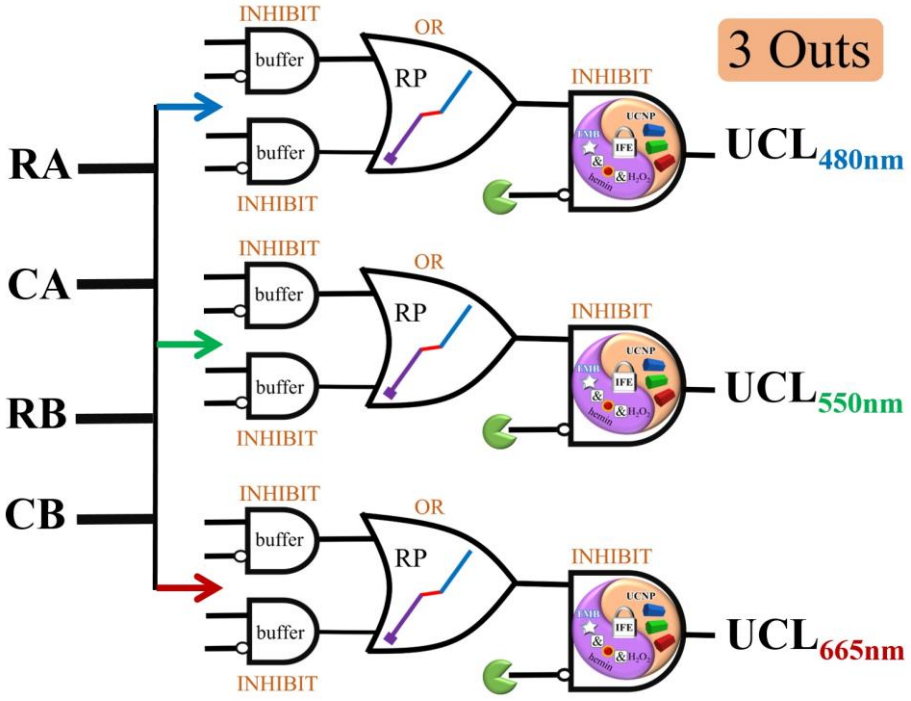

Figure S16. Triple-parallel-arrays derived from the 5-input concatenated logic circuit [INH/INH]-OR-INH.

References.

[S1]. L. Liang, Y. Liu, C. Bu, K. Guo, W. Sun, N. Huang, T. Peng, B. Sebo, M. Pan, W. Liu, S. Guo, X. Z. Zhao, Highly uniform, bifunctional core/double-shell-structured β-$NaYF_4$:Er^{3+}, Yb^{3+} @ SiO_2@TiO_2 hexagonal sub-microprisms for high-performance dye sensitized solar cells, *Adv. Mater.*, **2013**, 25, 2174-2180.

[S2]. D. Fan, K. Wang, J. Zhu, Y. Xia, Y. Han, Y. Liu, E. Wang, DNA-based visual majority logic gate with one-vote veto function, *Chem. Sci.*, **2015**, 6, 1973-1978;

[S3]. D. Fan, E. Wang, S. Dong, A DNA-based parity generator/checker for error detection through data transmission with visual readout and an output-correction function, *Chem. Sci.*, **2017**, 8, 1888-1895.

[S4]. D. Fan, E. Wang, S. Dong, An intelligent universal system yields double results with half the effort for engineering a DNA "Contrary Logic Pairs" library and various DNA combinatorial logic circuits, *Mater. Horiz.*, **2017**, 4, 924-931.

[S5]. D. Fan, J. Zhu, Q. Zhai, E. Wang, S. Dong, Cascade DNA logic device programmed ratiometric DNA analysis and logic devices based on a fluorescent dual-signal probe of a G-quadruplex DNAzyme, *Chem. Commun.*, **2016**, 52, 3766-3769.

[S6]. F. Wang, X. Liu, Recent advances in the chemistry of lanthanide-doped upconversion nanocrystals, *Chem. Soc. Rev.*, **2009**, 38, 976-989.